

Scalpel-SAM: A Semi-Supervised Paradigm for Adapting SAM to Infrared Small Object Detection

Zihan Liu*, Xiangning Ren†, Dezhang Kong‡, Yipeng Zhang§, and Meng Han‡

*School of Computer Science, Chengdu University, Chengdu, 610106, China

†China University of Geosciences, Beijing, China

‡Zhejiang University, Hangzhou, China

§Intelligent Computing Infrastructure Innovation Center, Zhejiang Lab, Hangzhou, China

Abstract—Infrared small object detection urgently requires semi-supervised paradigms due to the high cost of annotation. However, existing methods like SAM face significant challenges of domain gaps, inability of encoding physical priors, and inherent architectural complexity. To address this, we designed a Hierarchical MoE Adapter consisting of four white-box neural operators. Building upon this core component, we propose a two-stage paradigm for knowledge distillation and transfer: (1) Prior-Guided Knowledge Distillation, where we use our MoE adapter and 10% of available fully supervised data to distill SAM into an expert teacher (Scalpel-SAM); and (2) Deployment-Oriented Knowledge Transfer, where we use Scalpel-SAM to generate pseudo labels for training lightweight and efficient downstream models. Experiments demonstrate that with minimal annotations, our paradigm enables downstream models to achieve performance comparable to, or even surpassing, their fully supervised counterparts. To our knowledge, this is the first semi-supervised paradigm that systematically addresses the data scarcity issue in IR-SOT using SAM as the teacher model.

Index Terms—Semi-Supervised Learning, Infrared Small Object Detection, Segment Anything Model

I. INTRODUCTION

Infrared small object detection (IR-SOT) serves as a foundational technology in defense security, disaster rescue, and other critical areas, owing to its unique capability to identify thermal signatures under all-weather conditions and in total darkness where visible light systems fail [1], [2]. However, IR-SOT is being plagued by two major bottlenecks: First, infrared images have extremely minute targets, low signal-to-noise ratios, and a severe lack of textural cues and color cues that are abundant in natural images[1]. Second, obtaining pixel-level ground truth annotations incurs an exceedingly high cost [2]. The laborious and challenging process of manual labeling makes traditional methods, which rely on large-scale supervision, impractical. As such, exploring how to achieve efficient detection in the face of scarce data has become an urgent demand in this field.

Large foundation models, exemplified by Segment Anything Model (SAM)[3], offer a solution to this impasse. This is because SAM’s unique prompt-driven architecture can handle minimal, sparse guidance and output high-quality, dense segmentation masks. However, SAM was not designed for the specific physical properties of IR-SOT. Therefore, when we attempt to directly apply it to this specialized task, there are three challenges that must be addressed: (1) severe performance failure due to the domain gap, as visually demonstrated

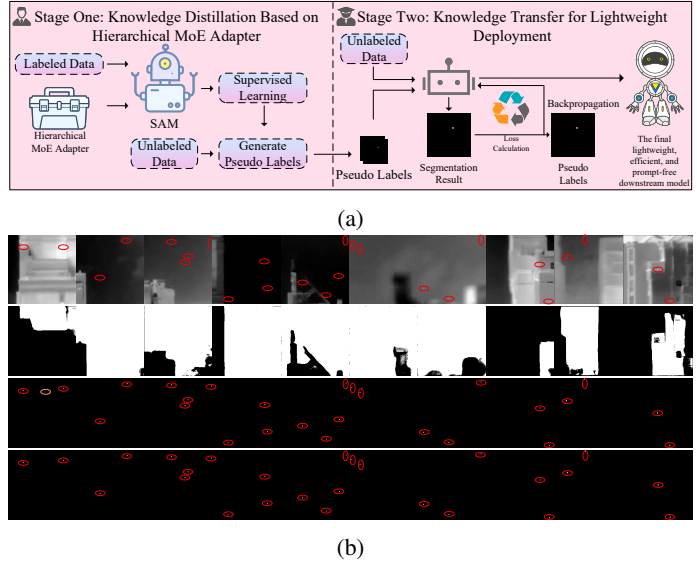


Fig. 1: The proposed paradigm and the visual evidence of the challenge. (a) Our two-stage paradigm. Stage One refines SAM (robot icon) into an expert teacher via our MoE adapter; Stage Two trains a lightweight student model (white robot) using teacher-generated pseudo-labels. (b) Visual comparison on the SIRST3 dataset. From top to bottom, the rows display: the original image, the generic SAM’s segmentation, our Scalpel-SAM’s precise result, and the GT.

in Figure 1b, where generic SAM (second row) produces noisy and failed segmentations; (2) the black-box limitations of Parameter-Efficient Fine-Tuning (PEFT) which prevent encoding physical priors; and (3) the inherent architectural complexity of SAM.

To systematically address these three challenges, we propose a two-stage knowledge distillation and transfer paradigm, as shown in Figure 1a. The Stage One addresses challenges 1 and 2, where we design an innovative Hierarchical MoE Adapter to fine-tune SAM into an expert teacher called Scalpel-SAM. Its core is an expert toolkit composed of four white-box neural operators (Physics-Informed Manifold Diffusion Operator (PIMDO), Spectral Prism Decoupler (SPD), Hyper-Parameterized Local Statistics Modulator (HPLSM), Topology-Guided Deformable Sampler (TGDS)). These oper-

ators explicitly encode anisotropic diffusion, frequency decoupling, local statistical adaptation, and topological connectivity priors into the network structure, elevating PEFT from a generic black-box into an interpretable regulator with surgical precision. The Stage Two tackles challenge 3, where we use the expert teacher trained in the first stage and generate high-quality pseudo labels. This pivotal step both amplifies the knowledge learned from the 10% supervised data and enables the knowledge to be transferred to a lightweight, efficient, and prompt-free student model, thereby drastically reducing the final deployment cost. This paradigm successfully transfers SAM’s powerful prior knowledge into a deployable lightweight model while solving the dual dilemmas of model capability and data costs.

Extensive experiments validate the efficacy of our paradigm. The results demonstrate that by applying our paradigm, the performance of downstream models approaches or **even surpasses that of their fully supervised counterparts**. To our knowledge, no prior semi-supervised paradigm in IR-SOT has managed to close this performance gap, let alone exceed the fully supervised upper bound. We also publish our code on [https://anonymous.4open.science/r/Scalpel-SAM\(Anonymized for review\)](https://anonymous.4open.science/r/Scalpel-SAM(Anonymized for review)). The contributions of this paper can be summarized as follows:

- We propose a two-stage knowledge distillation and transfer paradigm, which can automatically label vast data and help train downstream models. To our knowledge, this is the first semi-supervised learning paradigm for IR-SOT detection.
- We design a Hierarchical MoE Adapter that replaces the generic black-box structure of traditional PEFT methods with a domain-principle-driven expert toolkit, which can mimic a human expert’s progressive thought chain for target analysis and elevate PEFT into a domain-driven, highly interpretable adaptive regulator.
- Comprehensive experiments demonstrate that our paradigm approaches or even surpasses fully supervised performance using only 10% of the labeled data.

II. METHODOLOGY

For clarity, all mathematical symbols and notations used in our methodology are shown in Table I.

A. Overview: Knowledge Distillation and Transfer Paradigm

Our paradigm decouples the complex adaptation and learning process into two distinct stages.

1) *Stage One: Knowledge Distillation Based on Hierarchical MoE Adapter*: The goal of this stage is to utilize a minimal amount of all available fully supervised data D_L to refine the general SAM into an expert pseudo label generator Scalpel-SAM. To achieve this, we inject a Hierarchical MoE Adapter \mathcal{A}_θ into the last two Transformer modules following the ViT encoder \mathcal{E}_Φ of SAM. During fine-tuning, only the adapter parameters θ are updated, while the vast backbone

TABLE I: Symbols and Notations

Symbol	Description
Models, Data, and General Parameters	
D_L, D_U	Supervised (labeled) and unsupervised (unlabeled) datasets
D_{pseudo}	Generated pseudo label dataset
\mathcal{E}_Φ	Frozen SAM ViT Encoder backbone
Φ	Frozen parameters of \mathcal{E}_Φ
\mathcal{A}_θ	Trainable MoE Adapter with parameters θ
θ^*	Trainable parameters of \mathcal{A}_θ (in Stage One)
θ^{*+}	Optimized parameters of \mathcal{A}_θ after Stage One training
\mathcal{A}_{θ^*}	Expert teacher adapter with optimized parameters θ^{*+}
\mathcal{S}_ψ	Lightweight downstream student model
ψ	Trainable parameters of \mathcal{S}_ψ (in Stage Two)
I, M^{gt}	Input infrared image and its Ground Truth label
M_{pseudo}	Pseudo label generated by the teacher model
M_{pred}	Segmentation prediction output (from teacher or student model)
Core Component: MoE Adapter	
\mathcal{B}_l	l -th Transformer module
x_l	Input features to the l -th layer
$\mathcal{A}^{(l)}$	Adapter module injected into the l -th layer
$\mathcal{R}(\cdot)$	Dynamic routing network of the MoE
$\mathcal{E}_i(\cdot)$	i -th white-box expert operator
K	Total number of experts (K=4)
w_i	Weight assigned to the i -th expert by the router
$c(\cdot)$	Learnable intelligent diffusion controller in PIMDO
$\mathcal{W}_{ana}, \mathcal{W}_{syn}$	Learnable wavelet analysis and synthesis transforms in SPD
$\mathcal{M}_{spec}(\cdot)$	Spectral attention module in HPLSM
$\mathcal{H}_\psi(\cdot)$	Hypernetwork in HPLSM
$(\gamma_{ij}, \beta_{ij})$	Dynamically generated affine parameters by HPLSM
$\mathcal{G}_{off}(\cdot)$	Offset field prediction network in TGDS
Loss Functions	
\mathcal{L}_{total}	Total loss for Stage One
\mathcal{L}_{main}	Main segmentation task loss (BCE + Dice)
$\mathcal{L}_{BCE}, \mathcal{L}_{Dice}$	Binary Cross-Entropy loss and Dice loss
\mathcal{L}_{sparse}	Auxiliary sparsity loss for MoE
\mathcal{L}_{topo}	Topological regularization loss in TGDS
$\lambda_{bce}, \lambda_{dice}$	Weights for BCE and Dice losses
λ_{topo}	Weight for the topological loss
λ_{sparse}	Weight for the sparsity loss
f_i, P_i	Selection frequency and average probability of expert i in \mathcal{L}_{sparse}

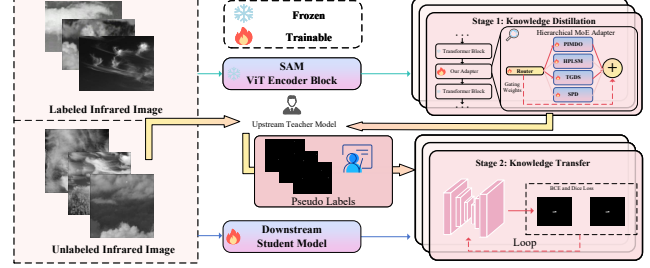


Fig. 2: The architecture of our two-stage paradigm. Stage 1 (Top-Right): Our trainable Hierarchical MoE Adapter (containing a router and four expert operators: PIMDO, SPD, HPLSM, TGDS) is injected into the frozen SAM ViT Encoder. Stage 2 (Bottom-Right): The resulting expert teacher generates pseudo labels from unlabeled data to supervise a lightweight downstream student.

network parameters Φ of SAM remain frozen. This process can be formalized as:

$$\theta = \arg \min_{\theta} \mathcal{L}_{task}(\mathcal{E}_\Phi(I; \mathcal{A}_\theta), M^{gt}), \quad \forall (I, M^{gt}) \in D_L \quad (1)$$

2) *Stage Two: Knowledge Transfer for Lightweight Deployment*: The goal of this stage is to distill knowledge from the expert teacher into an efficient, deployable, and prompt-free downstream model \mathcal{S}_ψ . We denote the optimized expert adapter from Stage One as \mathcal{A}_{θ^*} . This adapter is first used to generate pseudo-masks (M_j^{pseudo}) for the entire training set D_U . This yields a complete pseudo label dataset, D_{pseudo} , which then serves as the sole supervision to train the lightweight network \mathcal{S}_ψ from scratch.

B. Stage One: Knowledge Distillation Based on Hierarchical MoE Adapter

The complete training procedure of Stage One is detailed in Algorithm 1, and its architecture is illustrated in Figure 2.

Algorithm 1 Stage 1: Knowledge Distillation via Hierarchical MoE Adapter

Require: Frozen SAM ViT Encoder \mathcal{E}_Φ , Trainable MoE Adapter \mathcal{A}_θ (with Router \mathcal{R}_θ and Experts $\mathcal{E}_\theta^{(i)}$), Small fully supervised dataset $D_L = \{(I, M^{gt})\}$, Sparsity weight λ_{sparse} .
Ensure: Trained adapter parameters θ^* .
1: $\theta \leftarrow \text{InitializeAdapterParameters}()$
2: **for** each epoch **do**
3: **for** each $(I, M^{gt}) \in D_L$ **do**
4: $x \leftarrow \text{PatchEmbed}(I)$
5: **for** $l = 1$ to L **do**
6: $x_{block_out} \leftarrow \mathcal{B}_l(x)$
7: **if** $l > L - 2$ **then**
8: $x_{in} \leftarrow x$
9: $w \leftarrow \mathcal{R}_\theta(x_{in})$ (See Section II-B1)
10: $\mathcal{A}^{(l)}(x_{in}) \leftarrow 0$
11: **for** $i = 1$ to $K = 4$ **do**
12: $\mathcal{A}^{(l)}(x_{in}) \leftarrow \mathcal{A}^{(l)}(x_{in}) + w_i \cdot \mathcal{E}_\theta^{(i)}(x_{in})$
(See Section II-B1 & II-B2)
13: $x \leftarrow x_{block_out} + \mathcal{A}^{(l)}(x_{in})$ (See Section II-B2)
14: **else**
15: $x \leftarrow x_{block_out}$
16: $M_{pred} \leftarrow \text{Decoder}(x)$
17: $\mathcal{L}_{main} \leftarrow \mathcal{L}_{BCE}(M_{pred}, M^{gt}) +$
 $\mathcal{L}_{Dice}(M_{pred}, M^{gt})$ (See Section II-B3)
18: $\mathcal{L}_{sparse} \leftarrow \text{LoadBalancingLoss}(w)$
(See Section II-B3)
19: $\mathcal{L}_{total} \leftarrow \mathcal{L}_{main} + \lambda_{sparse} \cdot \mathcal{L}_{sparse}$
(See Section II-B3)
20: Update(θ)
21: **return** θ^*

1) *Dynamic Expert Routing Mechanism*: We employ a lightweight routing network $\mathcal{R}(\cdot)$ to dynamically compute weights w_i for our K parallel experts. We adopt a soft selection mechanism, where the final adapter output is a weighted fusion of all expert outputs $\mathcal{E}_i(x_l)$. Full formulas are provided in the supplementary material §A-A.

2) *White-Box Expert Toolbox*: The four neural operators we designed collectively mimic the progressive cognitive chain by which human experts analyze infrared images: (1) Signal Refining, separating suspicious signals from complex backgrounds (PIMDO & SPD); (2) Contextual Confirmation, determining signal authenticity based on local context (HPLSM); and (3) Morphological Focusing, delineating the target shape (TGDS).

• **Physics-Informed Manifold Diffusion Operator (PIMDO)**
To mimic the first step of this chain (refining signals), we propose the PIMDO operator, which we formulate as a learnable anisotropic diffusion process. Its continuous form is governed by the PDE:

$$\frac{\partial x}{\partial t} = \nabla \cdot (c(|\nabla x|) \nabla x) \quad (2)$$

The core of PIMDO is an intelligent diffusion controller $c(\cdot)$, which is trained to promote smoothing in regions with gentle gradients (i.e., noise) while suppressing diffusion at the steep gradients of target edges. However, operating solely in the

spatial domain is insufficient. In IR-SOT tasks, many high-frequency background clutter exhibit spatial features highly similar to real targets.

• **Spectral Prism Decoupler (SPD)** We propose the SPD operator, which aims to decouple the feature map into orthogonal subspaces $\{z_j\}$, representing different scales and frequency information, using a learnable wavelet-like transform \mathcal{W}_{ana} . Then, a spectral attention module $\mathcal{M}_{spec}(\cdot)$ automatically identifies and enhances the subspaces most likely to contain the target signal while suppressing those that contain clutter. Finally, the feature map is reconstructed through the inverse transform \mathcal{W}_{syn} :

$$x'_l = \mathcal{W}_{syn}(\{\alpha_j z_j\}_{j=1}^J), \quad \text{where } \alpha = \mathcal{M}_{spec}(\{z_j\}) \quad (3)$$

However, static decoupling fails in the highly dynamic and non-homogeneous backgrounds of infrared images (e.g., sky vs. ground clutter), which necessitates the adaptive mechanism introduced next.

• **Hyper-Parameterized Local Statistics Modulator (HPLSM)** This operator endows standard convolutions with environmental awareness capabilities. It contains a hypernetwork $\mathcal{H}_\psi(\cdot)$, which analyzes the local statistics of the input feature x_l in real-time and dynamically generates an affine transformation parameter pair $(\gamma_{ij}, \beta_{ij})$ for each spatial location (i, j) . These parameters then modulate the output of a shared base convolution kernel Conv_θ :

$$\text{Output}(x_l)_{ij} = \gamma_{ij} \odot \text{Conv}_\theta(x_l)_{ij} + \beta_{ij} \quad (4)$$

At this point, the target signal has been largely refined, but precise localization in the final step remains a challenge.

• **Topology-Guided Deformable Sampler (TGDS)** We design the TGDS, which employs an offset field prediction network $\mathcal{G}_{off}(\cdot)$, allowing deformable convolutions to actively and non-grid-like capture the target. More importantly, we introduce a crucial topological regularization term \mathcal{L}_{topo} , which encourages the sampled points $p_k + \Delta p_k$ to form a continuous structure that aligns with the target's geometric shape. The overall offset learning objective is:

$$\mathcal{L}_{offset} = \mathcal{L}_{task} + \lambda_{topo} \cdot \mathcal{L}_{topo}(p_k + \Delta p_k) \quad (5)$$

3) *Training Objectives*: The total loss \mathcal{L}_{total} consists of a main task loss \mathcal{L}_{main} and an auxiliary sparsity loss \mathcal{L}_{sparse} . The main loss is a standard weighted sum of BCE and Dice:

$$\mathcal{L}_{main} = \lambda_{bce} \cdot \mathcal{L}_{BCE}(M_{pred}, M_{gt}) + \lambda_{dice} \cdot \mathcal{L}_{Dice}(M_{pred}, M_{gt}) \quad (6)$$

The sparsity loss \mathcal{L}_{sparse} is a standard load balancing loss to encourage expert specialization:

$$\mathcal{L}_{sparse} = \alpha \cdot K \sum_{i=1}^K f_i \cdot P_i \quad (7)$$

where f_i and P_i are the selection frequency and average probability for expert i , respectively. The final weighted loss is:

$$\mathcal{L}_{total} = \mathcal{L}_{main} + \lambda_{sparse} \cdot \mathcal{L}_{sparse} \quad (8)$$

TABLE II: Performance comparison. **Green numbers** represent our paradigm’s results that exceed the SOTA point-supervised paradigm. For those results that even surpass the fully supervised paradigm, we use **red numbers** to highlight them.

Scheme	Description	SIRST3-Test				NUAA-SIRST-Test				NUDT-SIRST-Test				IRSTD-1K-Test			
		<i>mIoU</i>	<i>nIoU</i>	P_d	F_a												
ACM[4]	DLN Full	62.52	62.36	93.09	32.27	67.36	66.25	92.02	28.881	68.89	69.61	97.25	11.283	63.05	57.06	89.23	30.233
	DLN Course + PAL	50.4	51.71	92.29	30.338	55.33	56.61	85.67	27.89	53.83	52.67	92.60	18.31	30.58	41.76	78.45	18.295
	Ours	56.9 (91%)	54.37	92.89	28.641	61.81 (92%)	59.69	87.45	32.791	60.23 (87%)	61.42	93.65	21.578	65.26 (104%)	59.23	92.26	36.705
ALCNet[5]	DLN Full	64.35	66.22	93.02	30.97	69.25	67.49	92.45	14.82	64.96	63.26	96.61	12.547	62.78	56.47	90.57	36.135
	DLN Course + PAL	43.91	48.44	87.51	18.243	27.99	31.06	70.72	8.095	55.63	54.80	90.20	39.83	12.52	15.63	34.34	1.537
	Ours	61.78 (96%)	64.1	96.01	49.457	52.02 (75%)	53.01	83.65	56.877	63.51 (98%)	62.62	95.51	15.673	61.3 (98%)	55.53	90.36	15.680
MLCL-Net[6]	DLN Full	79.79	82.97	95.81	15.598	70.88	73.25	93.92	44.728	94.36	93.96	99.05	2.689	65.12	64.42	91.92	15.619
	DLN Course + PAL	64.28	69.55	94.95	24.652	67.35	69.67	94.30	48.638	73.38	74.3	96.72	19.993	59.89	58.32	90.24	18.922
	Ours	71.24 (89%)	75.00	95.95	32.839	72.09 (102%)	72.74	95.06	28.744	75.56 (80%)	76.85	98.08	15.326	64.39 (99%)	63.31	92.26	18.713
ALCL-Net[7]	DLN Full	69.22	70.59	93.49	36.973	64.22	65.24	93.92	67.572	65.54	62.73	90.91	49.515	66.46	62.53	87.21	41.525
	DLN Course + PAL	63.61	67.97	95.15	21.438	57.21	57.6	85.17	30.322	68.84	70.84	98.41	11.996	51.52	56.85	89.56	27.842
	Ours	70.84 (102%)	73.92	94.68	21.402	59.88 (93%)	59.74	91.63	48.775	71.08 (108%)	73.57	95.77	26.427	64.15 (97%)	62.47	91.58	19.947
DNANet[8]	DLN Full	81.56	85.12	96.15	10.417	69.39	72.6	94.68	62.084	85.95	87.00	98.52	9.973	63.75	63.06	90.24	19.472
	DLN Course + PAL	64.31	70.33	95.02	12.366	64.98	89.73	25.108	67.75	66.66	69.76	97.67	6.71	47.82	50.46	81.48	29.777
	Ours	73.34 (90%)	76.98	95.95	27.531	73.82 (106%)	73.26	93.54	17.15	72.68 (85%)	76.06	97.46	26.289	68.03 (107%)	61.48	87.88	17.157
GGL-Net[9]	DLN Full	80.89	84.16	97.54	13.296	70.82	71.56	94.68	43.63	67.72	64.97	93.60	32.396	65.96	64.14	93.80	32.415
	DLN Course + PAL	63.57	69.58	94.49	16.844	51.86	52.12	84.79	47.266	66.73	68.32	96.93	12.754	42.49	47.47	83.84	28.126
	Ours	70.55 (87%)	73.84	95.55	28.091	72.48 (102%)	72.47	95.44	22.981	71.29 (107%)	73.68	96.51	27.369	64.03 (97%)	63.97	91.92	12.867
UIUNet[10]	DLN Full	81.64	84.56	97.21	13.838	60.24	67.13	87.83	34.575	90.61	91.30	99.56	7.724	69.66	63.29	90.24	14.955
	DLN Course + PAL	37.24	39.02	71.50	32.099	36.93	39.19	84.41	10.815	75.5	76.35	99.05	6.894	52.98	51.60	92.26	33.08
	Ours	74.01 (91%)	77.20	96.68	22.548	73.19 (121%)	71.17	93.54	18.316	76.20 (84%)	77.29	99.61	6.752	68.65 (99%)	62.18	87.88	13.759
MSDA-Net[11]	DLN Full	83.52	86.44	97.61	20.824	67.89	69.12	92.02	40.818	91.27	91.55	98.41	3.217	70.87	65.11	92.93	14.291
	DLN Course + PAL	68.01	70.74	96.21	30.654	50.5	52.70	81.37	21.541	71.44	73.03	98.10	4.596	46.65	50.11	88.89	29.531
	Ours	73.28 (88%)	76.28	96.01	25.004	64.02 (94%)	63.99	90.87	30.596	75.10 (82%)	76.37	98.37	5.622	65.67 (93%)	64.58	92.26	23.42

C. Stage Two: Knowledge Transfer for Lightweight Deployment

While the expert teacher model from Stage One solves the Challenges 1 and 2, its massive size make it completely unsuitable for practical deployment (Challenge 3). Therefore, we designed Stage Two, with the target of transferring the knowledge from the upstream teacher model into a lightweight, efficient, and prompt-free downstream model \mathcal{S}_ψ .

1) *Pseudo Label Generation by Expert Teacher*: We employ the expert teacher to generate pseudo-masks M_j^{pseudo} for the entire dataset $D_{all} = D_L \cup D_U$, treating even labeled samples as unlabeled by disregarding their ground truths. For each image I_j , we perform a forward pass to obtain the pseudo label:

$$M_j^{pseudo} = \mathcal{E}_\Phi(I_j; \mathcal{A}_{\theta^*}) \quad (9)$$

Thus, we construct a large pseudo label dataset $D_{pseudo} = (I_j, M_j^{pseudo})_{j=1}^M$, which will serve as the sole source of supervision for the downstream model.

2) *Downstream Model Training*: After obtaining the pseudo label dataset D_{pseudo} , we select a lightweight network \mathcal{S}_ψ suitable for IR-SOT as the downstream student model. We train this downstream model \mathcal{S}_ψ from scratch, enabling it to learn to fit the pseudo labels generated by the expert teacher.

3) *Optimization Objective Update*: During the training process of the second stage, we only use the main task loss \mathcal{L}_{main} . This loss function is designed to minimize the difference between the predicted mask M_{pred} of the downstream model \mathcal{S}_ψ and the pseudo label M_{pseudo} generated by the expert teacher. As in stage one, \mathcal{L}_{main} is the weighted sum of BCE and Dice loss:

$$\mathcal{L}_{main} = \lambda_{bce} \cdot \mathcal{L}_{BCE}(M_{pred}, M_{pseudo}) + \lambda_{dice} \cdot \mathcal{L}_{Dice}(M_{pred}, M_{pseudo}) \quad (10)$$

where $M_{pseudo} \in D_{pseudo}$. It is worth noting that the auxiliary sparsity loss \mathcal{L}_{sparse} is no longer used here, as the MoE adapter does not participate in the training of this stage.

III. EXPERIMENT

A. Implementation Details

We conduct experiments on four public datasets: SIRST3 [12], NUAA-SIRST [4], NUDT-SIRST [8], and IRSTD-1K

[13]. We employ standard metrics $nIoU$, $mIoU$, P_d , F_a and our performance recovery rate : the performance ratio of our 10% data method against the 100% data baseline—to quantify data efficiency.

We compare our two-stage semi-supervised paradigm (using 10% data) against two key baselines: (1) the fully supervised paradigm as a theoretical upper bound, and (2) the SOTA point-supervised paradigm, PAL [14].

We apply these paradigms to eight SOTA model (ACM [4], ALCNet [5], MLCL-Net [6], ALCL-Net [7], DNANet [8], GGL-Net [9], UIUNet [10], and MSDA-Net [11]). We use PyTorch with a ViT-h SAM backbone and train on 8×A100-80G GPUs. All implementation details and hyperparameters are provided in the Supplementary Material.

B. Results

1) *Validation of Paradigm Necessity*: To validate our two-stage design, we benchmark against two pivotal baselines in Table III: (A) Direct Training on 10% Data: Training the student from scratch using only the 10% labeled subset (D_L) leads to significant performance drops. This confirms that 10% data is statistically insufficient for learning robust representations, inevitably causing overfitting. Our method circumvents this by using the expert teacher to propagate knowledge to unlabeled data, effectively amplifying the supervision signal. (B) Teacher Inference: Remarkably, our lightweight student matches or even surpasses the heavy Scalpel-SAM teacher. This demonstrates successful knowledge transfer: the student effectively internalizes the teacher’s complex physical priors into a compact representation, resolving the dilemma between model capability and deployment efficiency.

2) *Comparison with Fully Supervised Methods*: As quantified in Table II, our paradigm demonstrates exceptional data efficiency. Surprisingly, using only 10% of labeled data, our method not only approaches but also surpasses the performance of fully supervised counterparts. **Notably, the performance under fully supervised training is often regarded as an upper bound. To date, no other semi-supervised paradigm has approached, let alone exceeded this fully supervised baseline.** We attribute this breakthrough to two

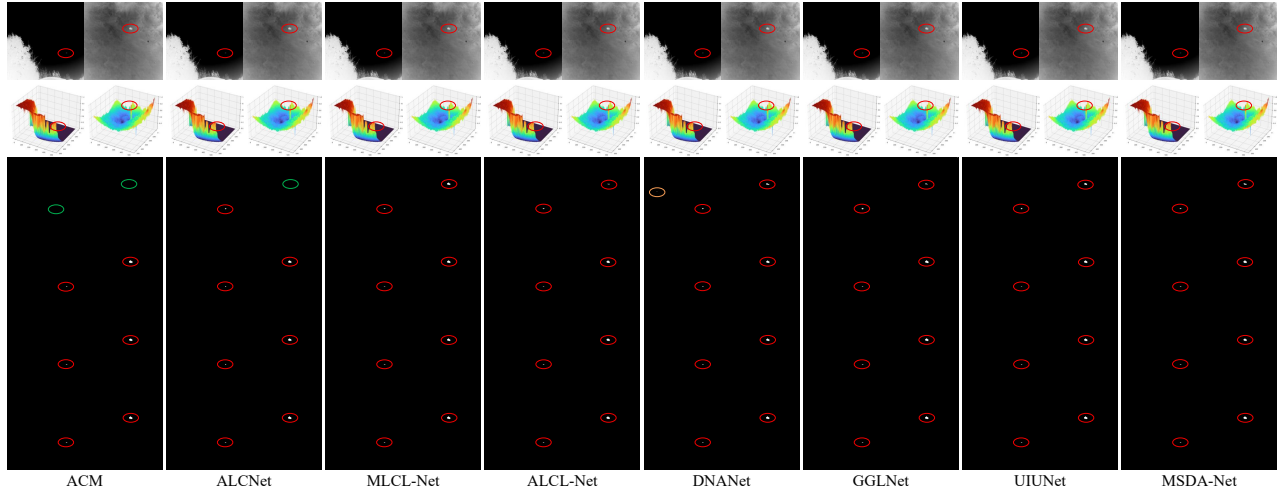


Fig. 3: Qualitative comparison on the IRSTD-1K dataset. Each row from top to bottom displays: the original infrared image, the 3D brightness map of the original image, the results of PAL, the results of the fully supervised method, the results of our method, and the ground truth (GT). For the predictions in this figure, red represents true positives (TP), orange represents false positives (FP), and green represents false negatives (FN). The visual results show that our method significantly outperforms PAL in terms of performance and achieves results that are close to, or even surpass, those of the fully supervised method.

factors: (1) Leveraging SAM’s robust pre-trained knowledge instead of training from scratch on scarce data; and (2) The MoE Adapter’s physical priors, which generate cleaner pseudo-labels by mitigating manual annotation noise. In addition, in Figure 3, we present qualitative comparisons of segmentation results produced by different methods.

3) Ablation Study:

a) Advancement of MoE routing and white-box expert Design: Table IV validates our core adapter design. The results confirm two key points: (1) Dynamic routing significantly outperforms the static average fusion baseline; and (2) our white-box experts substantially outperform generic black-box PEFT baselines (SAM-Adapter, LoRA). This proves the fundamental advantage of our domain-driven design.

b) Expert combination effectiveness analysis: We ablated the combination of our four white-box experts, as shown in Table VIII. The results confirm their complementarity: removing any single expert degrades performance, while the full four-expert model (All) achieves the best results.

c) Ablation of adapter insertion layers: We ablated the adapter insertion position and number, as shown in Table IX. The experiments confirm our design choice: inserting the MoE Adapter only after the last two ViT blocks yields the best balance of performance and cost. Notably, inserting adapters after all ViT layers performed the poorest, likely because disrupting SAM’s foundational features at shallow layers.

d) Ablation of Sparsity Loss Weight (λ_{sparse}): We conducted an ablation experiment on the weight coefficient λ_{sparse} of the auxiliary sparsity loss. As shown in Table X, the chosen value of $\lambda_{\text{sparse}} = 0.0100$ achieves the optimal performance balance across all datasets.

IV. RELATED WORK

Our work is closely related to IR-SOT [1] and PEFT [15]. The mainstream methods of IR-SOT have evolved from early local contrast measures (LCM) [16] to deep learning-based segmentation networks (such as DNANet [8] and UIUNet [17]). However, most of these methods follow the training from scratch paradigm, failing to leverage the priors of large foundational models and heavily relying on expensive pixel-level annotations. On the other hand, PEFT techniques have been successfully applied to adapt SAM [18]. However, these methods are generally universal black boxes that do not account for the unique physical properties of infrared images during adaptation.

V. CONCLUSION

We proposed a two-stage knowledge distillation and transfer paradigm to adapt foundation models to specialized, data-scarce domains. This paradigm first refines SAM into an expert teacher (Scalpel-SAM) using our novel Hierarchical MoE Adapter, which is composed of four white-box physical operators. It then transfers this knowledge to a lightweight, prompt-free downstream model. Experiments show this achieves or surpasses fully supervised SOTA performance with only 10% of labeled data. More importantly, the domain-principle-driven PEFT methodology we propose offers a promising pathway for extending the capabilities of foundational models to other specialized domains, such as medical imaging.

REFERENCES

[1] Mingjing Zhao et al., “Single-frame infrared small-target detection: A survey,” *IEEE Geosci. Remote Sens. Mag.*, vol. 10, no. 2, pp. 87–119, 2022.

TABLE III: Ablation study on the necessity of the two-stage paradigm. Our complete paradigm significantly outperforms two key baselines, demonstrating the immense value of first distilling an expert teacher and then performing transfer.

Scheme	Description	SIRST3-Test				NUAA-SIRST-Test				NUDT-SIRST-Test				IRSTD-1K-Test			
		$mIoU$	$nIoU$	P_d	F_a	$mIoU$	$nIoU$	P_d	F_a	$mIoU$	$nIoU$	P_d	F_a	$mIoU$	$nIoU$	P_d	F_a
ACM[4]	DLN Semi	*	*	*	*	*	*	*	*	25.61	23.15	51.64	83.188	51.96	48.61	90.24	68.475
ALCNet[5]	DLN Semi	2.17	1.2	5.05	3.042	64.30	63.09	88.59	29.224	24.80	23.72	72.38	94.586	9.26	5.68	23.57	32.036
MLCL-Net[6]	DLN Semi	53.63	59.70	86.84	64.991	72.44	72.34	95.44	21.746	48.60	57.21	83.49	84.429	60.58	59.46	93.27	32.947
ALCL-Net[7]	DLN Semi	48.80	51.61	83.32	51.966	65.27	65.87	90.49	36.564	44.28	51.39	82.01	118.554	57.98	53.80	90.57	67.184
DNA-Net[8]	DLN Semi	52.72	59.57	85.12	61.670	71.04	72.44	95.06	50.559	44.18	51.69	80.63	106.72	59.42	57.96	87.21	30.935
GG-Net[9]	DLN Semi	41.03	45.12	83.06	104.618	69.78	70.43	95.06	34.781	48.57	56.57	84.76	131.699	56.44	55.71	91.58	42.816
UIUNet[10]	DLN Semi	56.23	60.38	86.64	70.750	68.54	65.99	93.16	26.960	46.73	53.10	80.95	84.59	59.69	56.38	94.61	64.774
MSDA-Net[11]	DLN Semi	48.60	53.27	83.06	68.512	61.62	63.02	87.45	39.377	44.65	53.66	80.21	106.582	62.81	59.32	92.26	28.658
Ours (B)	DLN Semi	68.02	78.51	94.53	95.500	64.05	74.58	91.02	91.05	70.10	81.49	95.82	96.80	65.67	75.21	92.26	90.10
Ours(UIUNet)	DLN Semi	74.01	77.20	96.68	22.548	73.19	71.17	93.54	18.316	72.20	74.29	96.61	16.752	68.65	62.18	87.88	13.759

TABLE IV: A comprehensive ablation study on the routing mechanism, expert design, and adapter insertion strategy.

Variant	SIRST3-Test				NUAA-SIRST-Test				NUDT-SIRST-Test				IRSTD-1K-Test				
	$mIoU$	$nIoU$	P_d	F_a	$mIoU$	$nIoU$	P_d	F_a	$mIoU$	$nIoU$	P_d	F_a	$mIoU$	$nIoU$	P_d	F_a	
MoE Routing	Static (Avg. Fusion)	64.58	75.05	91.91	97.95	61.23	71.88	88.55	92.98	69.92	78.48	93.25	98.01	62.81	72.61	89.85	92.11
	Dynamic (Ours)	68.02	78.51	95.50	94.53	64.05	74.58	91.05	91.02	70.10	81.49	96.80	95.82	65.67	75.21	90.10	92.26
Expert Design	SAM-Adapter	62.13	72.88	90.05	98.51	59.98	70.35	87.21	94.13	65.25	76.91	92.07	98.85	61.39	71.05	88.52	93.04
	LoRA(t = 8)	65.52	76.54	93.61	95.92	62.48	73.01	89.54	92.15	68.31	79.88	94.63	97.18	64.03	73.77	90.88	91.04
	Black-box	63.45	74.01	91.52	97.33	60.71	71.24	87.95	93.58	66.19	77.80	92.74	98.42	62.18	71.89	89.21	92.65
	White-box (Ours)	68.02	78.51	95.50	94.53	64.05	74.58	91.05	91.02	70.10	81.49	96.80	95.82	65.67	75.21	90.10	92.26

TABLE V: Analysis of the white-box expert combination effectiveness.

Variant	SIRST3-Test				NUAA-SIRST-Test				NUDT-SIRST-Test				IRSTD-1K-Test			
	$mIoU$	$nIoU$	P_d	F_a	$mIoU$	$nIoU$	P_d	F_a	$mIoU$	$nIoU$	P_d	F_a	$mIoU$	$nIoU$	P_d	F_a
PI	62.15	72.93	98.55	90.18	58.39	68.95	95.31	85.78	63.92	75.15	98.99	91.53	60.23	69.91	94.19	87.25
SPD	62.51	73.28	98.21	90.45	58.77	69.31	94.98	86.03	64.29	75.48	98.73	91.88	60.65	70.32	93.88	87.61
HP	61.98	72.77	98.73	90.01	58.11	68.69	95.67	85.51	63.65	74.88	99.15	91.29	59.99	69.65	94.43	86.99
TG	63.02	73.75	97.88	90.91	59.13	69.72	94.51	86.49	64.81	76.01	98.41	92.25	61.12	70.79	93.45	88.04
PI + SPD	65.38	75.85	96.93	92.61	61.31	71.98	92.95	88.68	67.05	78.67	97.88	93.84	63.07	72.85	91.99	90.01
PI + HP	65.11	75.59	97.15	92.40	61.02	71.69	93.24	88.41	66.79	78.38	98.13	93.59	62.81	72.58	92.21	89.77
PI + TG	65.93	76.42	96.58	92.99	61.88	72.51	92.46	89.15	67.65	79.28	97.49	94.31	63.63	73.39	91.43	90.52
SPD + HP	65.45	75.93	96.89	92.68	61.39	72.05	92.88	88.75	67.13	78.74	97.81	93.91	63.15	72.93	91.91	90.08
SPD + TG	66.25	76.78	96.31	93.28	62.19	72.81	92.11	89.43	67.99	79.59	97.23	94.59	63.94	73.68	91.12	90.81
HP + TG	65.80	76.31	96.69	92.89	61.73	72.35	92.59	89.01	67.51	79.13	97.60	94.19	63.51	73.27	91.58	90.41
PI + SPD + HP	67.21	77.72	95.88	94.09	63.29	73.81	91.49	90.48	69.11	80.64	97.01	95.35	64.39	74.59	90.51	91.81
PI + HP + TG	67.59	78.08	95.65	94.31	63.65	74.19	91.18	90.79	69.53	81.01	96.85	95.59	65.31	74.89	90.29	92.05
All	68.02	78.51	95.50	94.53	64.05	74.58	91.05	91.02	70.10	81.49	96.80	95.82	65.67	75.21	90.10	92.26

TABLE VI: Ablation study on the Adapter insertion strategy.

Variant	SIRST3-Test				NUAA-SIRST-Test				NUDT-SIRST-Test				IRSTD-1K-Test			
	$mIoU$	$nIoU$	P_d	F_a	$mIoU$	$nIoU$	P_d	F_a	$mIoU$	$nIoU$	P_d	F_a	$mIoU$	$nIoU$	P_d	F_a
Last 1/2 ViT Layers	66.98	77.51	93.95	95.99	62.91	73.37	90.08	91.88	68.85	80.29	94.91	97.34	64.48	74.09	91.35	90.95
First 1/2 ViT Layers	65.55	76.16	92.77	96.81	61.85	72.28	88.98	92.71	67.57	79.05	93.68	98.01	63.53	73.21	90.37	91.78
All ViT Layers	60.57	71.15	88.62	99.53	58.72	68.85	85.62	95.93	63.96	75.32	90.47	99.34	60.01	69.55	86.87	94.21
Last 4 ViT Layers	67.67	78.15	94.28	95.71	63.62	74.11	90.67	91.35	69.69	81.06	95.45	96.99	65.25	74.87	91.97	90.43
None	35.12	48.29	75.33	132.15	33.48	45.91	71.88	158.29	38.21	50.78	78.41	141.33	34.03	46.59	73.51	162.51
Last 2 ViT Layers (Ours)	68.02	78.51	95.50	94.53	64.05	74.58	91.05	91.02	70.10	81.49	96.80	95.82	65.67	75.21	90.10	92.26

- [2] Renke Kou et al., “Infrared small target segmentation networks: A survey,” *PR*, vol. 143, pp. 109788, 2023.
- [3] Alexander Kirillov et al., “Segment anything,” in *ICCV*, 2023, pp. 4015–4026.
- [4] Yimian Dai et al., “Asymmetric contextual modulation for infrared small target detection,” in *WACV*, 2021, pp. 950–959.
- [5] Yimian Dai et al., “Attentional local contrast networks for infrared small target detection,” *TGRS*, vol. 59, no. 11, pp. 9813–9824, 2021.
- [6] Chuang Yu et al., “Infrared small target detection based on multiscale local contrast learning networks,” *Infrared Phys. Technol.*, vol. 123, pp. 104107, 2022.
- [7] Chuang Yu et al., “Pay attention to local contrast learning networks for infrared small target detection,” *GRSL*, vol. 19, pp. 1–5, 2022.
- [8] Boyang Li et al., “Dense nested attention network for infrared small target detection,” *TIP*, vol. 32, pp. 1745–1758, 2022.
- [9] Jinmiao Zhao et al., “Gradient-guided learning network for infrared small target detection,” *GRSL*, vol. 20, pp. 1–5, 2023.
- [10] Xin Wu et al., “Uiiu-net: U-net in u-net for infrared small object detection,” *IEEE TIP*, vol. 32, pp. 364–376, 2022.
- [11] Jinmiao Zhao et al., “Multi-scale direction-aware network for infrared small target detection,” *TGRS*, 2025.
- [12] Xinyi Ying et al., “Mapping degeneration meets label evolution: Learning infrared small target detection with single point supervision,” in *CVPR*, 2023, pp. 15528–15538.
- [13] Mingjin Zhang et al., “Isnet: Shape matters for infrared small target detection,” in *CVPR*, 2022, pp. 877–886.
- [14] Chuang Yu et al., “From Easy to Hard: Progressive Active Learning Framework for Infrared Small Target Detection with Single Point Supervision,” *arXiv preprint arXiv:2412.11154*, 2024.

- [15] James Kirkpatrick et al., “Overcoming catastrophic forgetting in neural networks,” *Proc. Nat. Acad. Sci.*, vol. 114, no. 13, pp. 3521–3526, 2017.
- [16] Yantao Wei et al., “Multiscale patch-based contrast measure for small infrared target detection,” *PR*, vol. 58, pp. 216–226, 2016.
- [17] Xin Wu et al., “Uiiu-net: U-net in u-net for infrared small object detection,” *TIP*, vol. 32, pp. 364–376, 2022.
- [18] Tianrun Chen et al., “Sam-adapter: Adapting segment anything in underperformed scenes,” in *ICCV*, 2023, pp. 3367–3375.

TABLE VII: Ablation experiment on the sparsity weight λ_{sparse} .

λ_{sparse}	SIRST3-Test				NUAA-SIRST-Test				NUDT-SIRST-Test				IRSTD-1K-Test			
	$mIoU$	$nIoU$	P_d	F_a	$mIoU$	$nIoU$	P_d	F_a	$mIoU$	$nIoU$	P_d	F_a	$mIoU$	$nIoU$	P_d	F_a
0.0010	67.18	77.65	96.45	93.81	63.13	73.69	93.61	90.15	69.19	80.59	96.98	94.98	64.73	74.25	91.89	91.31
0.0012	67.35	77.83	96.38	93.99	63.31	73.85	93.52	90.35	69.38	80.79	96.90	95.19	64.92	74.48	91.80	91.55
0.0014	67.51	78.00	96.30	94.13	63.50	74.05	93.43	90.56	69.59	81.01	96.81	95.40	65.13	74.70	91.71	91.78
0.0016	67.69	78.18	96.22	94.28	63.71	74.24	93.34	90.75	69.78	81.20	96.73	95.59	65.34	74.91	91.62	92.00
0.0018	67.85	78.35	96.13	94.41	63.89	74.42	93.24	90.89	69.95	81.37	96.67	95.72	65.52	75.08	91.51	92.15
0.0020	67.93	78.43	96.08	94.47	63.97	74.50	93.19	90.95	70.03	81.43	96.64	95.77	65.60	75.15	91.46	92.21
0.0040	67.98	78.47	96.06	94.50	64.01	74.54	93.17	90.98	70.06	81.46	96.63	95.79	65.63	75.18	91.44	92.23
0.0060	68.01	78.50	96.05	94.52	64.03	74.56	93.16	91.00	70.08	81.48	96.62	95.81	65.65	75.20	91.43	92.25
0.0080	68.02	78.51	96.04	94.53	64.04	74.57	93.15	91.01	70.09	81.49	96.62	95.82	65.66	75.21	91.42	92.26
0.0100 (Ours)	68.02	78.51	95.50	94.49	64.05	74.58	91.05	91.02	70.10	81.49	96.80	95.81	65.67	75.21	90.10	92.24
0.0400	67.81	78.29	96.15	94.35	63.82	74.33	93.28	90.80	69.88	81.27	96.75	95.63	65.45	75.00	91.58	92.06
0.0800	67.43	77.91	96.34	94.05	63.41	73.95	93.48	90.43	69.49	80.89	96.86	95.28	65.05	74.61	91.75	91.69

Supplementary Material for Scalpel-SAM: Precision Adaptation of SAM via Domain-Principle-Driven Expert Adapters

A. SUPPLEMENTARY DETAILS FOR METHODOLOGY

This document provides detailed formulas and implementation details omitted for brevity in the main paper §3 (Methodology).

A. Hierarchical MoE Adapter

a) *Adapter Integration*: For the l -th layer of the ViT encoder, the input features are x_l , and the output x_{l+1} after passing through the Transformer module \mathcal{B}_l and our adapter $\mathcal{A}^{(l)}$ is:

$$x_{l+1} = \mathcal{B}_l(x_l) + \mathcal{A}^{(l)}(x_l) \quad (11)$$

1) *Dynamic Expert Routing Mechanism*: The routing network $\mathcal{R}(\cdot)$ receives the input features $x_l \in \mathbb{R}^{N \times C}$ of the layer and computes the gating weights $\mathbf{w} \in \mathbb{R}^K$ for the K experts via a small MLP:

$$\mathbf{w} = \text{Softmax}(\mathbf{W}_2 \cdot \text{ReLU}(\mathbf{W}_1 \cdot \text{GAP}(x_l) + \mathbf{b}_1) + \mathbf{b}_2) \quad (12)$$

where $\text{GAP}(\cdot)$ is the global average pooling operation. We employ a Soft Selection mechanism, where the outputs of all experts $\mathcal{E}_i(x_l)$ are weighted and fused to obtain the final feature adjustment:

$$\mathcal{A}^{(l)}(x_l) = \sum_{i=1}^K w_i \cdot \mathcal{E}_i(x_l) \quad (13)$$

2) “White-Box” Expert Toolbox: Detailed Implementation:

a) 1. *PIMDO*: The continuous form of the core idea of PIMDO is shown in Eq. (2) in the main paper. In the implementation, we numerically discretize it using the explicit forward Euler method. For any pixel $x_{i,j}$, its update in the $t+1$ iteration is given by:

$$x_{i,j}^{t+1} = x_{i,j}^t + \Delta t \cdot \nabla \cdot (c(|\nabla x_{i,j}^t|) \nabla x_{i,j}^t) \quad (14)$$

where the time step Δt is set to 0.2, and the gradient ∇x is approximated using a fixed 3x3 Sobel operator. This evolution process is iterated $T = 3$ times.

b) 2. *SPD*: Eq. (3) in the main paper shows the reconstruction process of SPD. The analysis filter bank \mathcal{W}_{ana} consists of a set of parallel, learnable 2D depthwise separable convolutions, which decompose the input features into $J = 4$ different frequency subspaces.

c) 3. *HPLSM*: Eq. (4) in the main paper shows the modulation process of HPLSM. The hypernetwork $\mathcal{H}_\psi(\cdot)$ inside it is a small convolutional neural network consisting of two 3x3 convolutional layers, a global average pooling layer, and a final fully connected layer.

d) 4. *TGDS*: Eq. (5) in the main paper shows the topological-aware learning objective of TGDS. The core topological loss \mathcal{L}_{topo} is a regularization term based on local consistency, which enforces a topological constraint by penalizing the difference between the pixel prediction $M_{pred}(i, j)$ and the average probability of its four neighbors $\mathcal{N}_4(i, j)$. The mathematical definition is as follows:

$$\mathcal{L}_{topo} = \frac{1}{HW} \sum_{i,j} \left| M_{pred}(i, j) - \frac{1}{|\mathcal{N}_4(i, j)|} \sum_{\mathbf{p}' \in \mathcal{N}_4(i, j)} M_{pred}(\mathbf{p}') \right| \quad (15)$$

B. SUPPLEMENTARY DETAILS FOR EXPERIMENTS

This document provides the implementation details and additional ablation experiments omitted for brevity in the main paper §4 (Experiment).

A. Implementation Details

We implement our model based on the PyTorch framework. The backbone of SAM uses the ViT-h version, pre-trained on ImageNet-1K. In Stage One (Knowledge Distillation), we use the AdamW optimizer to train the hierarchical expert mixture adapter for 100 epochs with a batch size of 32. The initial learning rate is set to e^{-3} , and we adopt a cosine annealing strategy. In Stage Two (Knowledge Transfer), we choose SOTA models such as ACM, DNANet, and UIUNet as downstream segmentation networks, also training with the AdamW optimizer for 400 epochs with a batch size of 16. All experiments are conducted on 8x A100-80G GPUs.

C. DETAILED COMPONENT ABLATIONS

A. Expert Combination Effectiveness Analysis

We performed detailed ablation experiments on the combination of the four ‘white-box’ experts to validate the indispensability of each expert. As shown in Table VIII, we started with the full four-expert model, sequentially removed individual experts, and tested the performance of different expert combinations. The experimental results clearly show that removing any single expert results in a performance decline, and the full four-expert combination achieved the best performance, proving the complementarity and systematic design of our experts.

B. Ablation of Adapter Insertion Layers

The number and placement of Adapter insertions in different layers of SAM’s ViT encoder have a significant impact on the experimental results. We conducted ablation experiments on the insertion position and number of Adapters, with results

TABLE VIII: Analysis of the Effectiveness of the 'White-Box' Expert Combination. The full four-expert combination yields the best performance, and removing any individual expert leads to a performance decline, demonstrating the complementarity of our design.

Variant	SIRST3-Test				NUAA-SIRST-Test				NUDT-SIRST-Test				IRSTD-1K-Test			
	IoU	$nIoU$	P_d	F_a	IoU	$nIoU$	P_d	F_a	IoU	$nIoU$	P_d	F_a	IoU	$nIoU$	P_d	F_a
PI	62.15	72.93	98.55	90.18	58.39	68.95	95.31	85.78	63.92	75.15	98.99	91.53	60.23	69.91	94.19	87.25
SPD	62.51	73.28	98.21	90.45	58.77	69.31	94.98	86.03	64.29	75.48	98.73	91.88	60.65	70.32	93.88	87.61
HP	61.98	72.77	98.73	90.01	58.11	68.69	95.67	85.51	63.65	74.88	99.15	91.29	59.99	69.65	94.43	86.99
TG	63.02	73.75	97.88	90.91	59.13	69.72	94.51	86.49	64.81	76.01	98.41	92.25	61.12	70.79	93.45	88.04
PI + SPD	65.38	75.85	96.93	92.61	61.31	71.98	92.95	88.68	67.05	78.67	97.88	93.84	63.07	72.85	91.99	90.01
PI + HP	65.11	75.59	97.15	92.40	61.02	71.69	93.24	88.41	66.79	78.38	98.13	93.59	62.81	72.58	92.21	89.77
PI + TG	65.93	76.42	96.58	92.99	61.88	72.51	92.46	89.15	67.65	79.28	97.49	94.31	63.63	73.39	91.43	90.52
SPD + HP	65.45	75.93	96.89	92.68	61.39	72.05	92.88	88.75	67.13	78.74	97.81	93.91	63.15	72.93	91.91	90.08
SPD + TG	66.25	76.78	96.31	93.28	62.19	72.81	92.11	89.43	67.99	79.59	97.23	94.59	63.94	73.68	91.12	90.81
HP + TG	65.80	76.31	96.69	92.89	61.73	72.35	92.59	89.01	67.51	79.13	97.60	94.19	63.51	73.27	91.58	90.41
PI + SPD + HP	67.21	77.72	95.88	94.09	63.29	73.81	91.49	90.48	69.11	80.64	97.01	95.35	64.99	74.59	90.51	91.81
PI + HP + TG	67.59	78.08	95.65	94.31	63.65	74.19	91.18	90.79	69.53	81.01	96.85	95.59	65.31	74.89	90.29	92.05
All	68.02	78.51	95.50	94.53	64.05	74.58	91.05	91.02	70.10	81.49	96.80	95.82	65.67	75.21	90.10	92.26

TABLE IX: Ablation study on the Adapter insertion strategy.

Variant	SIRST3-Test				NUAA-SIRST-Test				NUDT-SIRST-Test				IRSTD-1K-Test			
	mIoU	nIoU	P_d	F_a	mIoU	nIoU	P_d	F_a	mIoU	nIoU	P_d	F_a	mIoU	nIoU	P_d	F_a
Last 1/2 ViT Layers	66.98	77.51	93.95	95.99	62.91	73.37	90.08	91.88	68.85	80.29	94.91	97.34	64.48	74.09	91.35	90.95
First 1/2 ViT Layers	65.55	76.16	92.77	96.81	61.85	72.28	88.98	92.71	67.57	79.05	93.68	98.01	63.53	73.21	90.37	91.78
All ViT Layers	60.57	71.15	88.62	99.53	58.72	68.85	85.62	59.93	63.96	75.32	90.47	99.34	60.01	69.55	86.87	94.21
Last 4 ViT Layers	67.67	78.15	94.28	95.71	63.62	74.11	90.67	91.35	69.69	81.06	95.45	96.99	65.25	74.87	91.97	90.43
None	35.12	48.29	75.33	132.15	33.48	45.91	71.88	158.29	38.21	50.78	78.41	141.33	34.03	46.59	73.51	162.51
Last 2 ViT Layers (Ours)	68.02	78.51	95.50	94.53	64.05	74.58	91.05	91.02	70.10	81.49	96.80	95.82	65.67	75.21	90.10	92.26

TABLE X: Ablation experiment on the sparsity weight λ_{sparse} .

λ_{sparse}	SIRST3-Test				NUAA-SIRST-Test				NUDT-SIRST-Test				IRSTD-1K-Test			
	IoU	$nIoU$	P_d	F_a	IoU	$nIoU$	P_d	F_a	IoU	$nIoU$	P_d	F_a	IoU	$nIoU$	P_d	F_a
0.0010	67.18	77.65	96.45	93.81	63.13	73.69	93.61	90.15	69.19	80.59	96.98	94.98	64.73	74.25	91.89	91.31
0.0012	67.35	77.83	96.38	93.99	63.31	73.85	93.52	90.35	69.38	80.79	96.90	95.19	64.92	74.48	91.80	91.55
0.0014	67.51	78.00	96.30	94.13	63.50	74.05	93.43	90.56	69.59	81.01	96.81	95.40	65.13	74.70	91.71	91.78
0.0016	67.69	78.18	96.22	94.28	63.71	74.24	93.34	90.75	69.78	81.20	96.73	95.59	65.34	74.91	91.62	92.00
0.0018	67.85	78.35	96.13	94.41	63.89	74.42	93.24	90.89	69.95	81.37	96.67	95.72	65.52	75.08	91.51	92.15
0.0020	67.93	78.43	96.08	94.47	63.97	74.50	93.19	90.95	70.03	81.43	96.64	95.77	65.60	75.15	91.46	92.21
0.0040	67.98	78.47	96.06	94.50	64.01	74.54	93.17	90.98	70.06	81.46	96.63	95.79	65.63	75.18	91.44	92.23
0.0060	68.01	78.50	96.05	94.52	64.03	74.56	93.16	91.00	70.08	81.48	96.62	95.81	65.65	75.20	91.43	92.25
0.0080	68.02	78.51	96.04	94.53	64.04	74.57	93.15	91.01	70.09	81.49	96.62	95.82	65.66	75.21	91.42	92.26
0.0100 (Ours)	68.02	78.51	95.50	94.53	64.05	74.58	91.05	91.02	70.10	81.49	96.80	95.82	65.67	75.21	90.10	92.26
0.0400	67.81	78.29	96.15	94.35	63.82	74.33	93.28	90.80	69.88	81.27	96.75	95.63	65.45	75.00	91.58	92.06
0.0800	67.43	77.91	96.34	94.05	63.41	73.95	93.48	90.43	69.49	80.89	96.86	95.28	65.05	74.61	91.75	91.69

shown in Table IX. The experiments indicate that inserting our MoE Adapter only after the last two ViT blocks achieves the best balance between performance and cost (i.e., "Last 2 ViT Layers (Ours)"). The performance is poorest when the Adapter layers are inserted after all ViT layers, likely due to excessive shallow-layer adapters disrupting SAM's general foundational features.

C. Ablation of Sparsity Loss Weight (λ_{sparse})

We conducted an ablation experiment on the weight coefficient λ_{sparse} of the auxiliary sparsity loss. As shown in Table X, the chosen value of $\lambda_{sparse} = 0.0100$ achieves the optimal performance balance across all datasets.